

# Spatially dispersive transport: A mesoscopic phenomenon in disordered organic semiconductors

Noam Rappaport, Yevgeni Preezant, and Nir Tessler\*

*Microelectronic & Nanoelectronic Centers, Electrical Engineering Department, Technion Israel Institute of Technology, Haifa 32000, Israel*

(Received 25 June 2007; published 26 December 2007)

We present time-of-flight-type calculations of the transport master equation applied to thin film disordered materials. We show that the energetic disorder in conjunction with a thin film results in electronic inhomogeneity. This inhomogeneity manifests itself as dispersive transport which can be described as a linear sum of close to normal-transport paths. Namely, in thin films of disordered materials the transport parameters do not converge to the infinite sample parameters but present a dispersive mesoscopic phenomenon. By defining a spatial distribution function of the charge velocity (mobility) we are able to examine the effect of the degree of disorder and film thickness on the electronic inhomogeneity. We postulate that in a given sample the spatial distribution characteristic of holes and the one characteristic of electrons are most likely nonidentical. Hence, in organic thin-film light-emitting diodes the energetic disorder is a limiting factor concerning charge recombination and efficiency.

DOI: [10.1103/PhysRevB.76.235323](https://doi.org/10.1103/PhysRevB.76.235323)

PACS number(s): 73.61.Jc

## INTRODUCTION

The issue of charge transport in disordered organic semiconductors has been studied for a few decades<sup>1–8</sup> by now. The evolution of organic light-emitting diodes (OLEDs) and organic field-effect transistors (FETs) has triggered attempts to provide a single physical picture<sup>7,9–12</sup> through the use of implicit models. In a recent paper by Preezant and Tessler<sup>13</sup> it was argued that many of the implicit models fail to describe well current organic LEDs since they do not account for the electric-field-induced carrier-heating phenomenon. It was also mentioned<sup>13</sup> that in the infinite sample limit, regardless of the model used, the interpretation of the simulated (calculated) charge transport in terms of a mobility value is ill defined for a high degree of disorder ( $\sigma > 5kT$ ) where the transport becomes spatially inhomogeneous. We have recently suggested that thin-film devices exhibit a new type of mesoscopic physical phenomenon<sup>8,14</sup> that was not captured by the previously existing models simply because these models *a priori* assumed an infinite sample. In this paper we use time-resolved master equation transport calculations to provide better rigor to the mobility spatial distribution function concept.<sup>8,14</sup>

In previous papers we showed that for films that are very thin ( $\sim 100$  nm) in the direction of propagation but infinite in the other two dimensions one can describe the transport as being composed of many parallel mobility or current paths which are randomly distributed and give rise to the mobility spatial distribution function<sup>8,14</sup> (MDF) or more generally to a velocity distribution function (VDF). At first glance this may look like going back to the earlier days where there were many arguments<sup>15</sup> whether one should describe the transport in disordered materials as made of parallel paths, serial paths, or something in between.<sup>16,17</sup> Those works were largely concerned with providing a global picture for transport in amorphous materials as presented by an infinitely large sample. Here, however, we are concerned with a mesoscopic phenomenon where the transport parameters have not yet statistically converged towards the infinite sample

parameters. The choice of a parallel picture here is dictated solely by the asymmetry in the sample dimensions.

Before proceeding we need first to discuss the notion of a mobility value being meaningless or ill defined. To do that we need to establish what the mobility value is supposed to mean or what use do we want to make of it. In basic textbooks<sup>18,19</sup> it is shown that the mobility arises when one tries to reduce the transport phenomenon to a description that can be carried out by two parameters: mobility and diffusion. The motivation for this simplification is often presented as the need to describe (simulate) semiconductor devices:

$$J_h = qp\mu_h E - q \frac{\partial}{\partial x}(D_h p) = qp\mu_h E - qD_h \frac{\partial}{\partial x}p - qp \frac{\partial}{\partial x}D_h. \quad (1)$$

Equation (1) is the continuity equation where  $J_h$  is the hole current,  $p$  is the hole density,  $q$  is the elementary charge,  $E$  is the electric field,  $D_h$  is the hole diffusion constant, and  $\mu_h$  is the hole mobility value. This equation is typically coupled to the Poisson equation (2) to provide an adequate description of the device performance:

$$\epsilon_r \epsilon_0 \frac{\partial E}{\partial x} = p \cdot q. \quad (2)$$

Namely, for a mobility value to be meaningful one needs to be able to use it in equations of the form of Eq. (1) above and obtain a true description of the device under study. In modern devices where the resolution and dimensions are ever shrinking one expects from the set of equations (1) and (2) to reproduce the charge density, current, and the spatial distribution of both. Now we can relate to the suggestion that at high degree of disorder the mobility is meaningless or ill defined. In the paper by Yu *et al.*<sup>5</sup> it is shown (Fig. 5 in Ref. 5) that for a disorder parameter ( $\sigma$ ) slightly above 100 meV current patterns (filaments) evolve. It is obvious that Eqs. (1) and (2) cannot reproduce such patterns and hence, in the current context, the mobility extracted for such materials is meaningless. In a seminal paper by Scher and Montroll<sup>3</sup> they

used different arguments to show that in highly disordered systems the mobility is an ill-defined concept.

If one strictly applies the above discussion, then even whenever the mobility is charge density dependent it becomes an ill-defined concept. This is of course not practical since by introducing a density dependence in the form of  $\mu(p)$ , Eqs. (1) and (2) are again useful and do reproduce the physical picture. This teaches us that practically whenever it becomes possible to provide a functional form for the mobility it can be reinstated as a valid concept for certain, if not many, physical circumstances. We consider that establishing the MDF is a step towards making the mobility meaningful in mesoscopic thin-film disordered materials.

### NUMERICAL MODEL

To establish the concept of spatial distribution of the transport parameters we recall that the transport of charge carriers in amorphous organic semiconductors is modeled as hopping transport between localized states assuming specific energetic and spatial distribution functions. This physical framework has been studied for many years using different types of model formulations.<sup>1-4,7,20</sup> The Monte Carlo (MC) approach, promoted by Bassler *et al.*, established charge hopping in a Gaussian density of states as the most commonly accepted framework and indeed this has also been used in the master equation (ME) approach.<sup>5</sup>

The actual model used here is that of the ME approach, and for our numerical simulations we utilize a linearized form of the master equation that holds for low charge densities:

$$\frac{\partial}{\partial t} f_i(t) = - \sum_{j \neq i} W_{ji} f_i(t) + \sum_{j \neq i} W_{ij} f_j(t). \quad (3)$$

And the hopping rate that we use is the so called Miller-Abrahams rate:<sup>16</sup>

$$W_{ij} = \nu_0 \exp(-\gamma |R_{ij}|) \begin{cases} \exp[-(\varepsilon_j - \varepsilon_i)/kT] & \forall \varepsilon_j > \varepsilon_i, \\ 1, & \text{otherwise,} \end{cases} \quad (4)$$

where  $\nu_0 = 10^{12}$  Hz,  $\gamma = 10^8$  cm<sup>-1</sup>, and  $T = 300$  K. In our simulations, small-volume cubic lattices of sites are taken with a distance of 1 nm between the sites. The energy levels of the sites are then randomized according to a Gaussian density of states (DOS) of a specified standard deviation ( $\sigma$ ):

$$\text{DOS}(\varepsilon) = \frac{N_V}{\sqrt{2\pi}\sigma} \exp\left[-\left(\frac{\varepsilon - \varepsilon_0}{\sqrt{2}\sigma}\right)^2\right].$$

Simulations were carried out for Gaussian DOS distributions with three different standard deviations:  $\sigma = kT$ ,  $\sigma = 2kT$ , and  $\sigma = 3kT$ , where  $k$  is the Boltzmann constant and  $T$  was taken to be 300 K—i.e., room temperature. For each energy distribution and for every layer thickness in our chosen set (25, 50, and 75 nm), the site energy levels were randomized and the master equation was solved to produce the probability function for crossing the lattice. This procedure of randomizing the energies and solving the master equation

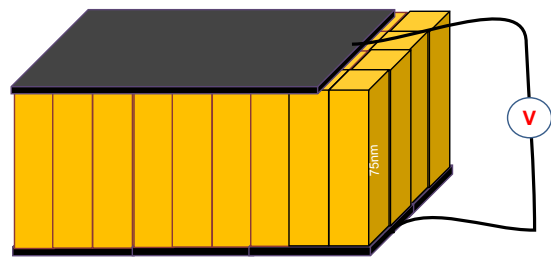


FIG. 1. (Color online) Schematic description of a thin film device “broken” into many mobility pathways.

was repeated several hundreds of times for every layer thickness and energy distribution. Each randomization step is equivalent to producing a new environment through which the carrier propagates.

The conventional use of creating many different lattices is to arrive at a statistically valid average of the transit time. Here, however, we are interested mainly in the standard deviation of transit times or to be exact in the mobility or velocity distribution function. The motivation here derives from the fact that in thin-film devices charge carriers that cross the device sample a very limited volume<sup>5,8</sup> the transport properties of which may be highly different depending on the position it is picked from in the sample plane. Namely, when we produce many environments we are actually trying to reconstruct the properties of a film by dividing it into many little rectangular pipes stretching across the layer thickness in a manner very similar to the way the electronic current would sample the film (see Fig. 1). In the following calculation results we wish to show the effect of the sample length and electronic disorder on the spread of transit times in the sample.

### RESULTS

In order to set the scene for our master equation calculations we start with simulations of the standard semiconductor equations [see Eqs. (1) and (2)] that represent a classic Gaussian transport with  $D/\mu = kT/q$ . One of the concerns with the interpretation, in terms of a mobility value, of a time-of-flight simulation (or measurement) carried out on thin films is the role of diffusion and the finite time it takes for the injected charges to take the expected steady state shape of a Gaussian packet moving across the device. To this end we plot in Fig. 2 the calculated current in response to a  $\delta$ -function (pulse) excitation close to the contact, thus mimicking ideal time-of-flight experiment. Due to the different conventions used in the literature, Fig. 2(a) is in linear scale and Fig. 2(b) is in log-log scale. The upper (solid) curve was calculated for electric field of  $2 \times 10^5$  V/cm and the lower (dashed) curve for  $5 \times 10^4$  V/cm (using  $\mu = 2 \times 10^{-7}$  cm<sup>2</sup>/V s). The sample length was chosen to be 75 nm. For  $2 \times 10^5$  V/cm we see a classical curve with a plateau indicating a motion under constant velocity (mobility) and a sharp drop indicating the arrival of the charge packet at the other end. We note that the curve for  $5 \times 10^4$  V/cm shows no plateau or a clear arrival

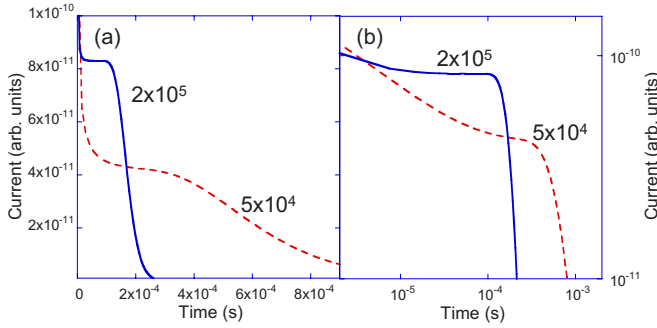


FIG. 2. (Color online) Calculated current in response to a  $\delta$ -function excitation close to the contact at  $t=0$ . The solid and dashed lines were calculated using  $\mu=2\times 10^{-7}$   $\text{cm}^2/\text{V s}$  and for electric fields of  $2\times 10^5$   $\text{V/cm}$  and  $5\times 10^4$   $\text{V/cm}$ , respectively. (a) Linear scale. (b) Log-log scale.

point due to the diffusion-induced broadening under low electric fields (and short samples).

It is commonly accepted that if the curve does not exhibit a clear plateau, it is not straightforward to extract a mobility value. This difficulty is associated with the fact that not all the carriers are moving at the same velocity or that the velocity of the charges exiting the device is time dependent. Since the mobility is supposed to be the average velocity, several methods have been suggested to extract it from such curves. Using the method of finding the cross point of the slopes<sup>21,22</sup> before and after charges have started to exit the device we get  $3\times 10^{-7}$   $\text{cm}^2/\text{V s}$  and  $2.5\times 10^{-7}$   $\text{cm}^2/\text{V s}$  for the electric fields of  $5\times 10^4$   $\text{V/cm}$  and  $2\times 10^5$   $\text{V/cm}$ , respectively. In a recent publication<sup>8,14</sup> we have introduced a method for extracting the distribution of the charge's velocity and dubbed it the MDF.<sup>8</sup> The method relies on differentiating the current response:

$$\frac{d^2 I(t)}{dt^2} = \frac{dJ(t)}{dt} = -\frac{APqd^2}{2Vt^3} g\left(\frac{d^2}{Vt}\right). \quad (5)$$

In the low-excitation-density (linear) regime  $J$  is the response to a pulse ( $\delta$ -function) excitation and  $I$  is the response to excitation in the form of a step function. In Eq. (5),  $A$ ,  $P$ , and  $q$  are constants,  $d$  is the sample length,  $V$  is the applied voltage,  $t$  is the time,  $\frac{d^2}{Vt} = \frac{v_t}{E}$  with  $v_t$  being the velocity of a carrier (pathway) transit time of  $t$ ,  $E$  the electric field, and  $g$  is the velocity distribution function.

Figure 3 describes the velocity distribution, presented in mobility units, which is derived by applying Eq. (5) to the data in Fig. 2. We note that the distribution is slightly asymmetric where the tail to larger values denotes the faster carriers that are being “pushed” forward by the diffusion current. Having found the VDF the representative mobility can now be calculated by finding the average of the VDF divided by the applied electric field:

$$\mu = \frac{\int g \frac{v}{E} d\left(\frac{v}{E}\right)}{\int g d\left(\frac{v}{E}\right)}. \quad (6)$$

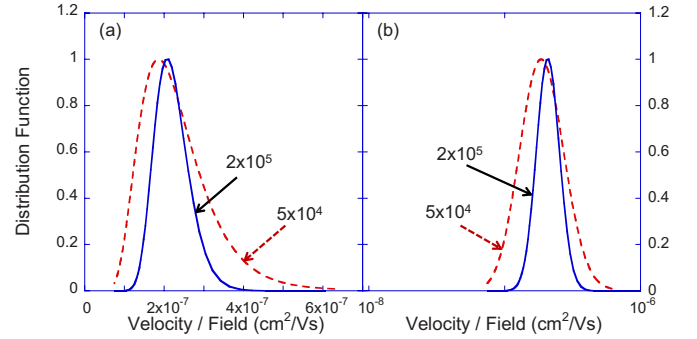


FIG. 3. (Color online) The velocity distribution function derived by applying Eq. (5) to the simulation data presented in Fig. 2. The dashed and solid lines are for electric fields of  $5\times 10^4$  and  $2\times 10^5$   $\text{V/cm}$ , respectively. (a) Linear  $x$  axis. (b) Log  $x$  axis.

Applying Eq. (6) to the VDFs shown in Fig. 3 we find a mobility value of  $2.3\times 10^{-7}$   $\text{cm}^2/\text{V s}$  and  $2.2\times 10^{-7}$   $\text{cm}^2/\text{V s}$  for the electric fields of  $5\times 10^4$   $\text{V/cm}$  and  $2\times 10^5$   $\text{V/cm}$ , respectively. Namely, this method of extracting the mobility from a transient curve is at least as good as other methods previously suggested. In the following we will use this method to define the mobility associated with a given path or transient curve.

After establishing the method for analyzing transient curves we move to examine transient curves produced by the microscopic master equation based simulations. Typical results of the output of the simulation program are shown in Fig. 4. The plot is for electric field of  $5\times 10^4$   $\text{V/cm}$  and results for  $\sigma=3kT$  and  $d=75$   $\text{nm}$  are shown. In the calculations shown here we do not exceed the field of  $1\times 10^5$   $\text{V/cm}$  since above this value the charge population becomes hotter than the lattice<sup>13</sup> and the transport becomes nonlinear with the applied field (i.e., less intuitive). The size of the box in the lateral dimension was taken to be  $9\times 9$   $\text{nm}^2$  and to avoid possible edge effects cyclic boundary conditions were used. The choice of 9 nm may seem far too small but for a normal organic LED operating under 2–5 V above the flatband condition the spread of a charge packet across 100 nm is  $\sim 10$  nm (assuming Gaussian propagation  $p(x,t) \propto e^{(x-\mu Et)^2/4Dht}$ ). Since the simulations are done in the low-charge-density limit, we ignore in this specific calculation (of 10 nm) the dependence of the Einstein relation on charge density which may enhance this value twofold to threefold.<sup>9</sup>

Figure 4(a) shows the current response to a  $\delta$ -function excitation at  $x=0$ , and Fig. 4(b) shows the current response for a step function excitation. The solid lines show the response of two individual paths, and the dashed line shows an average over a few hundreds of paths. Figures 4(c) and 4(d) are added to allow better understanding of the charge carrier dynamics behind the current response of the individual paths [solid lines in Figs. 4(a) and 4(b)]. Figure 4(c) shows on a log scale [to match the scale of Fig. 4(a)] the amount of charges in the path, presented as a % of the charges injected at  $t=0$ . We note that charges are starting to exit the path through the opposite contact only at times longer than  $10^{-4}$  s. This tells us that the current decrease at shorter times is due to fast charge relaxation towards local equilibrium at the vi-

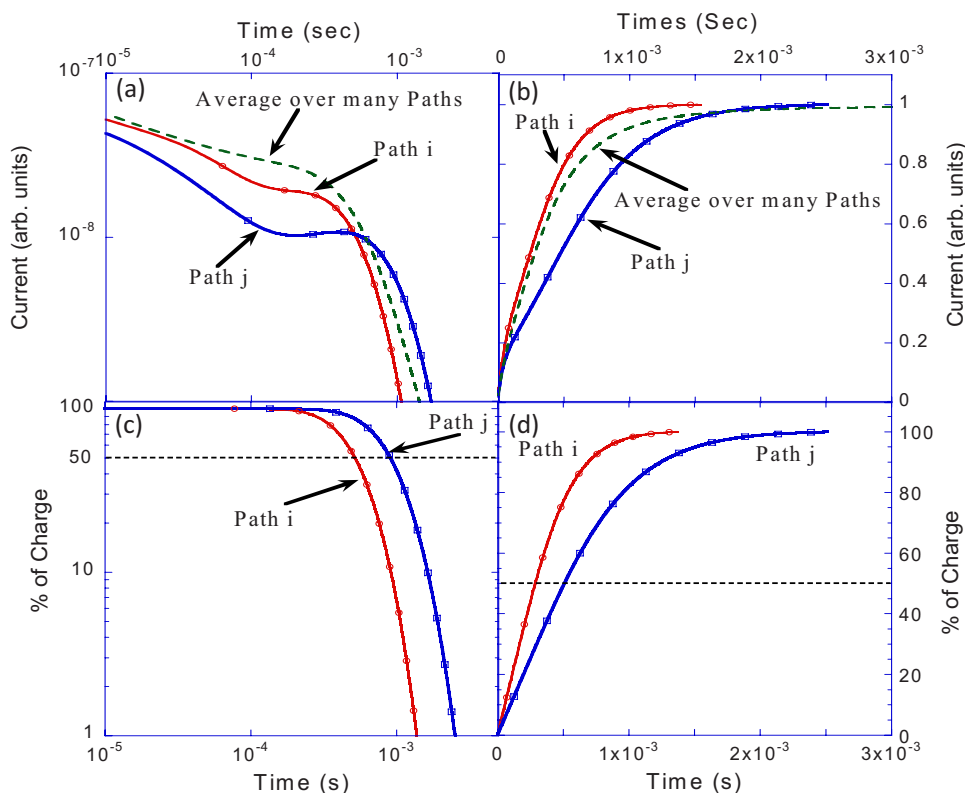


FIG. 4. (Color online) (a) Time-resolved current transient as a result of an impulse charge excitation at  $x=t=0$  (classical time of flight). (b) Time-resolved current transient as a result of a step function charge excitation. (c) The fraction of charges that is in the device following an impulse charge excitation at  $x=t=0$ . (d) The fraction of charges, relative to the steady-state value, which is in the device following a step function charge excitation.

cinity of the contact where charges were “optically” injected at  $t=0$ . The initial current decrease for the individual paths is followed by roughly a constant value until the point in time at which charges start reaching the other contact and exit the path. The existence of a plateau is also a random variable where in some of the paths it is pronounced and in some it is nonexistent. Figure 4(d) shows on a linear scale [to match the scale of Fig. 4(b)] the amount of charges in the path, presented as a % of the charges in the path at  $t=\infty$  following a step-function excitation (constant injection rate). Basically, Figs. 4(b) and 4(d) do not add information to that in Figs. 4(a) and 4(c) since there is a simple integral relation between the two. However, the linear scales used in Figs. 4(b) and 4(d) visually emphasize the last decade which takes up most of the transport time. Finally, the dashed lines in Figs. 4(a) and 4(b), which are representing the entire sample through a sum of few hundreds of paths, show no indication whatsoever of a dominant mobility/velocity value. We can thus state that the dispersive nature of the thin sample considered here at least partly arises from spatial variations of the mobility due to the finite volume sampled by a carrier traversing the thin film.

Next, we are interested in constructing the mobility distribution function of the entire sample and to test for its dependence on the disorder parameter and the film thickness.

Figure 5 shows the velocity distribution expressed as a mobility distribution, using  $v = \mu E$ , of the two paths shown in Fig. 4 as well as for the average over hundreds of paths which represents the response of a macroscopic device. The calculation uses Eq. (5) and is identical to that employed for Fig. 3. Comparing Figs. 5(a) and 3(a) we find the VDF of the two paths to be very similar to that resulting from classic

transport equations. Figure 5(b) shows that the two paths have a somewhat similar distribution function, only shifted with respect to each other. We also note that the device equivalent distribution develops a tail towards low values which is a result of the very slow paths existing in any disordered sample.

Once the velocity distribution function of each path (as in Fig. 5) is known, one can deduce the mobility of each path (defined as the average velocity) and thus produce the mobility distribution function of the entire device. Figure 6 shows the mobility distribution function (solid line) and the velocity distribution function (dashed line) of the simulated device ( $\sigma = 3kT$ ,  $E = 5 \times 10^4$  V/cm,  $d = 75$  nm). Unlike the VDF, the MDF excludes the effects due to charge diffusion

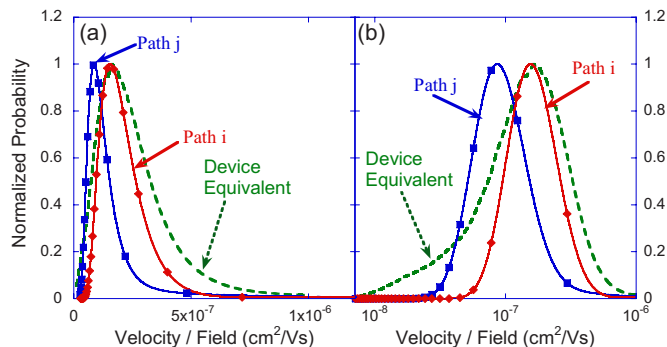


FIG. 5. (Color online) The velocity distribution function derived by applying Eq. (5) to the simulation data presented in Fig. 4(a). The velocity distribution function shown are for path  $i$  (diamond), path  $j$  (square), and for the average of many paths (dashed lines). (a) Linear scale. (b) Semilog  $x$  scale.

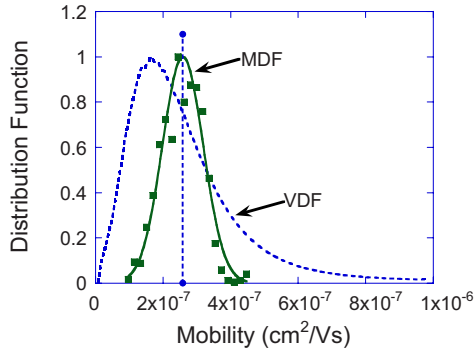


FIG. 6. (Color online) The device equivalent velocity distribution function (dashed line) and the device mobility distribution function (solid line and squares). The vertical line denotes the average of the velocity distribution function.

and hence it assumes a symmetric Gaussian-like shape.

After establishing the MDF and its relation to the velocity distribution function we can now move to examine closely the MDF and its dependence on material and device parameters. Since the MDF represents the electronic uniformity of the sample, we are actually examining the uniformity of the electronic properties across the device plane.

Figure 7 shows the calculated MDF for the same layer thickness and applied electric field ( $E=5 \times 10^4$  V/cm,  $d=75$  nm) but for three different disorder parameters of the Gaussian DOS ( $\sigma=1kT$ ,  $2kT$ ,  $3kT$ ). Figure 7(a) shows the well-known effect of the mobility dependence on the disorder parameter  $\sigma$  predicted for the infinite-sample case ( $\exp[-(c\sigma/kT)^2]$  with  $c \sim 0.67$ ).<sup>2,23</sup> Figure 7(b) shows the three MDFs where the  $x$  axis was normalized such that the peak of the distribution will occur at  $\mu=1$ . This figure shows that the width of the mobility distribution function, which is a relatively macroscopic parameter, is directly related to the energy disorder which is of a more microscopic nature. Namely, in a thin-film device the electronic disorder leads to electronic inhomogeneity across the device plane.

Finally, we examine the effect of the sample thickness on the sample's electronic inhomogeneity. Figure 8 shows the MDF calculated for three different film thickness:  $d=25 \mu\text{m}$  (diamonds),  $50 \mu\text{m}$  (squares), and  $75 \mu\text{m}$

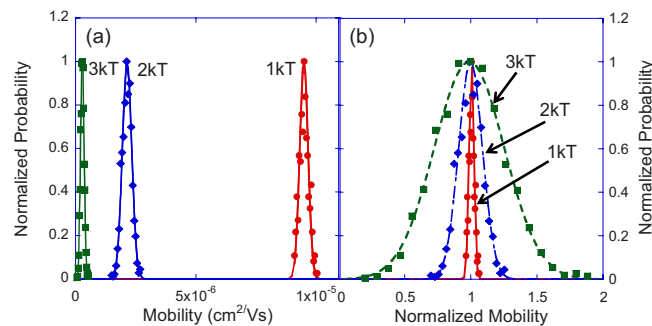


FIG. 7. (Color online) (a) The mobility distribution function for  $\sigma=1kT$  (circles),  $2kT$  (diamonds),  $3kT$  (squares). (b) The mobility distribution functions where the  $x$ -axis values were normalized such that the peaks of the MDFs coincide. As before,  $E=5 \times 10^4$  V/cm,  $d=75$  nm, and  $T=300$  K.

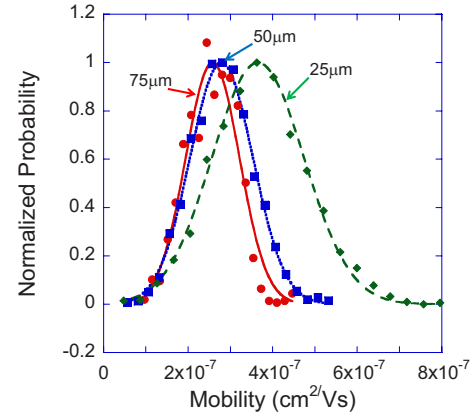


FIG. 8. (Color online) The mobility distribution function for  $\sigma=3kT$ ,  $E=5 \times 10^4$  V/cm, and  $d=25 \mu\text{m}$  (diamonds),  $50 \mu\text{m}$  (squares), and  $75 \mu\text{m}$  (circles).

(circles). As the film becomes thicker the volume sampled by a carrier crossing the device increases. In the infinite limit this volume would be large enough to reproduce the full Gaussian DOS and the starting position across the film plane would be irrelevant and the sample would be considered homogeneous. For the intermediate case (Fig. 8) we see the trend towards a homogenous sample where the width of the MDF is decreasing with increasing sample thickness. It also shows that as the sample becomes thicker, the very fast paths gradually disappear.

## DISCUSSION

Using the linearized master equation we have constructed a time-dependent simulation of the charge transport based on the so-called Miller-Abraham's hopping rate. By presenting the results as current transients we mimicked the time-of-flight experiment (Figs. 2 and 4). Our goal here was to examine whether disorder in the energy landscape may lead, in thin films, to spatial in-plane inhomogeneity in the transport properties. To this end we did not use the common approach of finding the average value over many different simulated volumes but rather displayed the distribution of values such that the variance could be examined as well. The quantity that the technologists among us would be interested in is the current or how uniform it is across a thin-film device.

By dividing the thin films into many boxes having the size of a typical volume a charge carrier would sample we were able to show that the transient curves are very different between different locations across the film. In order to analyze the current transients we translated them into a velocity distribution function following the formalism described in Ref. 8. Comparing the velocity distribution function derived from a fully Gaussian transport model [Eq. (1) and Fig. 3] to that of the device equivalent function (dashed line in Fig. 5) we find them to be very different in shape. Namely, the device as a whole cannot be represented using a single mobility and diffusion constant value. Examining the local transport or the velocity distribution function for a single path (solid lines Fig. 5) we find that the results are very similar to the Gaussian case but for a very slight enhancement of the high mo-

bility side tail. This implies that, to a good approximation, one can reproduce the curve of individual pathways using mobility and diffusion in their classical sense.

In our analysis we defined the mobility as the average velocity of the charge carriers crossing the film. This is equivalent to requiring that the steady-state current would be directly related to a single parameter  $\mu$  ( $I = \mu En$ ) or to requiring that the mobility distribution function would represent the current distribution function to be found in LED-type devices. Namely, in the general case where the disorder may be very high and/or the contributions of relaxation and diffusion to the steady-state current are not negligible then the results presented as mobility distribution function should be read as a current distribution function.

Using the above “definition” for the mobility we could derive the mobility (current) distribution function and examine the role of the disorder parameter ( $\sigma$ ) and the film thickness ( $d$ ). The results presented in Fig. 8 show that the larger the volume sampled by a charge carrier, the smaller is the spatial inhomogeneity of the transport properties (the current). Figure 7 shows that for a given volume sampled by the charge carrier (i.e., fixed travel length of 75 nm) the inhomogeneity is enhanced by the disorder and for  $\sigma = 3kT$  the full width at half maximum (FWHM) of the distribution is 30% of the mean value.

The results shown in Figs. 7 and 8 have several implications for the operation of thin-film devices such as OLEDs or solar cells. First, the variation in current density between different points across the device means that part of the molecules undergo oxidation and reduction significantly more than others which makes them more susceptible to degradation (the fast paths are the weak points as far as stability is concerned). Second, for a bipolar device, such as OLED, it is very likely that the characteristic distribution functions of electrons and holes currents are not identical, leading to incomplete spatial overlap between the currents and to reduced electroluminescence efficiency.<sup>24</sup> Namely, electronic disorder is a limiting factor in terms of device efficiency.

#### ACKNOWLEDGMENT

This research was supported by the Israel Science Foundation.

\*Corresponding author: nir@ee.technion.ac.il;  
www.ee.technion.ac.il/nir

<sup>1</sup>N. F. Mott, *Electronic Processes in Non-crystalline Materials* (Clarendon Press, Oxford, 1979).

<sup>2</sup>M. Van der Auweraer, F. C. Deschryver, P. M. Borsenberger, and H. Bassler, *Adv. Mater. (Weinheim, Ger.)* **6**, 199 (1994).

<sup>3</sup>H. Scher and E. M. Montroll, *Phys. Rev. B* **12**, 2455 (1975).

<sup>4</sup>S. V. Rakhmanova and E. M. Conwell, *Appl. Phys. Lett.* **76**, 3822 (2000).

<sup>5</sup>Z. G. Yu, D. L. Smith, A. Saxena, R. L. Martin, and A. R. Bishop, *Phys. Rev. B* **63**, 085202 (2001).

<sup>6</sup>V. I. Arkhipov, P. Heremans, E. V. Emelianova, G. J. Adriaenssens, and H. Bassler, *J. Phys.: Condens. Matter* **14**, 9899 (2002).

<sup>7</sup>Y. Roichman, Y. Preezant, and N. Tessler, *Phys. Status Solidi A* **201**, 1246 (2004).

<sup>8</sup>N. Rappaport, O. Solomesch, and N. Tessler, *J. Appl. Phys.* **99**, 064507 (2006).

<sup>9</sup>Y. Roichman and N. Tessler, *Appl. Phys. Lett.* **80**, 1948 (2002).

<sup>10</sup>S. Shaked, S. Tal, Y. Roichman, A. Razin, S. Xiao, Y. Eichen, and N. Tessler, *Adv. Mater. (Weinheim, Ger.)* **15**, 913 (2003).

<sup>11</sup>C. Tanase, E. J. Meijer, P. W. M. Blom, and D. M. de Leeuw, *Phys. Rev. Lett.* **91**, 216601 (2003).

<sup>12</sup>W. F. Pasveer, J. Cottaar, C. Tanase, R. Coehoorn, P. A. Bobbert, P. W. M. Blom, D. M. de Leeuw, and M. A. J. Michels, *Phys. Rev. Lett.* **94**, 206601 (2005).

<sup>13</sup>Y. Preezant and N. Tessler, *Phys. Rev. B* **74**, 235202 (2006).

<sup>14</sup>N. Rappaport, Y. Bar, O. Solomesch, and N. Tessler, *Appl. Phys. Lett.* **89**, 252117 (2006).

<sup>15</sup>H. Bassler (private communication).

<sup>16</sup>A. Miller and E. Abrahams, *Phys. Rev.* **120**, 745 (1960).

<sup>17</sup>S. Baranovski, *Charge Transport in Disordered Solids with Applications in Electronics*, Wiley Series in Materials for Electronic & Optoelectronic Applications (Wiley, West Sussex, 2006).

<sup>18</sup>S. Selberherr, *Analysis and Simulation of Semiconductor Devices* (Springer-Verlag, Wien, 1984).

<sup>19</sup>S. M. Sze, *Physics of Semiconductor Devices* (Wiley, New York, 1981).

<sup>20</sup>H. Bassler, G. Schonherr, M. Abkowitz, and D. M. Pai, *Phys. Rev. B* **26**, 3105 (1982).

<sup>21</sup>H. Scher, M. F. Shlesinger, and J. T. Bendler, *Phys. Today* **44**(1), 26 (1991).

<sup>22</sup>F. Laquai, G. Wegner, C. Im, H. Bassler, and S. Heun, *J. Appl. Phys.* **99**, 023712 (2006).

<sup>23</sup>V. I. Arkhipov, E. V. Emelianova, and G. J. Adriaenssens, *Phys. Rev. B* **64**, 125125 (2001).

<sup>24</sup>G. J. Adriaenssens and V. I. Arkhipov, *Solid State Commun.* **103**, 541 (1997).